Int J Mater Form (2016) 9:423–434
DOI 10.1007/s12289-015-1238-7

THEMATIC ISSUE: FLEXIBLE FORMING - INCREMENTAL SHEET FORMING & ROLL FORMING

A first step towards a simple in-line shape compensation routine for the roll forming of high strength steel

Buddhika Abeyrathna[1] · **Bernard Rolfe**[2] · **Peter Hodgson**[1] · **Matthias Weiss**[1]

Received: 28 August 2014 / Accepted: 31 March 2015 / Published online: 18 April 2015

Abstract The roll forming process is increasingly used in the automotive industry for the manufacture of structural and crash components from Ultra High Strength Steel (UHSS). Due to the high strength of UHSS (<1GPa) even small and commonly observed material property variations from coil to coil can result in significant changes in material yield and through that affect the final shape of the roll formed component. This requires the re-adjustment of tooling to compensate for shape defects and maintain part geometry resulting in costly downtimes of equipment. This paper presents a first step towards an in-line shape compensation method that based on the monitoring of roll load and torque allows for the estimation of shape defects and the subsequent re-adjustment of tooling for compensation. For this the effect of material property variation on common shape defects observed in the roll forming process as well as measurable process parameters such as roll load and torque needs to be understood. The effect of yield strength and material hardening on roll load and torque as well as longitudinal bow is investigated via experimental trials and numerical analysis. A regression analysis combined with Analysis of Variance (ANOVA) techniques is employed to establish the relationships between the process and material parameters and to determine their percentage influence on longitudinal bow, roll load and torque. The study will show that the level of longitudinal bow, one of the major shape defects observed in roll forming, can be estimated by variations in roll load and torque.

Keywords Roll forming · Sensitivity study · Longitudinal bow · Defect compensation · Roll load and torque

✉ Buddhika Abeyrathna
buddhika.a@research.deakin.edu.au

[1] Institute for Frontier Materials, Deakin University, Pigdons Rd., Waurn Ponds, VIC 3216, Australia

[2] School of Engineering, Deakin University, Pigdons Rd., Waurn Ponds, VIC 3216, Australia

Introduction

Ultra High Strength Steels (UHSS) are increasingly used in the automotive industry to reduce weight and improve passenger safety [1]. Their high material strength and low formability restrict the manufacture of UHSS with conventional forming methods such as stamping. One forming method that has been shown to enable the forming of high strength, low ductile materials to components with high accuracy is roll forming [2] and the process is increasingly used in the automotive industry for the manufacture of longitudinal components for structural and crash applications [1]. Roll forming has been shown to enable the forming of tighter forming radii [3] and shows a lower level of springback [4] compared to simple bending. This has been majorly related to the incremental nature of the process [4, 5] where the material is incrementally bent in successive roll forming stations. Additionally to that springback and shape defects can be flexibly compensated for by re-adjustment of the tooling [6] which is a major advantage when roll forming UHSS.

Previous studies have shown that even small changes in material yield can have a major effect on the process and the final shape of the roll formed components [7]. Most shape defects in roll forming are due to small permanent longitudinal deformation in the strip [8] and a reduction in yield stress reduces the resistance of the material for unwanted plastic deformation. This represents a major problem when forming UHSS where even small and common changes in material

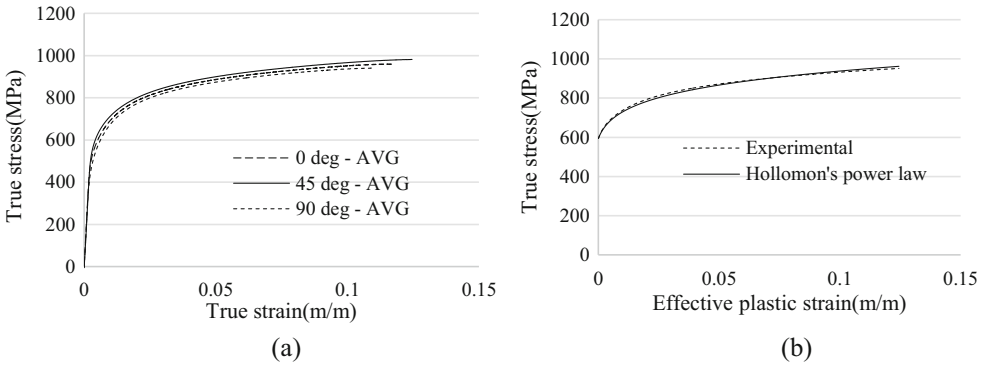

Fig. 1 **(a)** True stress strain curve of DP 780 steel for samples cut 0, 45 and 90° to the rolling direction **(b)** True stress effective plastic strain curve and the fit with the Hollomon's equation for DP780 steel

strength and hardening characteristic can lead to major variations in yield stress (10 % reduction in material strength for a material with $YP_{0.2\%}$=1000 MPa leads to a reduction in yield stress by 100 MPa [9]). This requires the re-adjustment of tooling to compensate for shape defects and maintain part geometry and results in costly equipment downtimes which are unacceptable in automotive engineering.

To enable the wide-spread application of the roll forming process in the automotive industry methods need to be developed that enable the compensation of shape defects without stopping the roll forming line. An inline shape compensation method would require the monitoring of process parameters that enable the estimation of material property variations in the process. Additionally to that the effect of changes in material properties on the final part shape needs to be known to re-adjust the tooling accordantly and compensate for shape defects. There are few defect compensation techniques recorded in the literature [10, 11]. Ona and Jimma [10] experimentally investigated a method to eliminate twist, bow and camber of symmetrical channel sections. They used an exit straightener, roll pressure adjustment, transverse shift of the rolls, over-bending of the strip and a twist forming stand as the correction methodologies. Their methodology is based on trial and error and it may not be practical especially when UHSS is formed as their material properties are continuously changing which would lead to frequent machine stoppages and readjustments. Groche et al. [11] introduced an in-line springback compensation method for high and ultra-high strength steel, where the part is over-bent for shape compensation in the last forming pass depending on the part shape measured just before the station. This requires a feedback signal which was taken from a set of laser sensors and cameras. This paper presents a first step toward an in-line shape compensation method that based on the monitoring of roll load and torque allows for the estimation of shape defects and the subsequent re-adjustment of tooling for compensation. For this the effect of material property variation on common shape defects observed in the roll forming process as well as measurable process parameters such as roll load and torque need to be understood.

Only a few investigations have analysed roll load and torque in the roll forming process and revealed that both parameters are a function of material yield [12, 13]. Bhattacharyya et al. [12] introduced a semi empirical method to calculate the roll load by equating the external work to the total deformation work (bending and stretching). A trapezoidal channel section was taken into account for the investigation. According to their investigation, roll load is a function of yield strength, material thickness, fold angle and the flange length while experimental and statistical work performed by Lindgren [13] showed that roll load and torque depend on material yield strength, forming angle and material thickness. Work performed by Abeyrathna et al.[7] on the roll forming of a trapezoidal section suggested that roll load and torque are not only a function of material yield, but also depend on material hardening which is an important aspect given that some UHSS such as DP1000 steel show very high initial hardening rates [14].

A numerical study performed by Azizitafti et al.[15] observed that longitudinal bow decreases with increasing yield strength of the roll formed material and this has been verified by experimental work performed by Abeyrathna et al.[7]. This suggests that it may be possible to directly estimate the level of longitudinal bow in a roll formed section by directly monitoring the change in roll forming load and torque during the process.

Table 1 Material properties of DP780

Material	Yield Strength(MPa)	Young's Modulus(GPa)	Ultimate tensile strength(MPa)	Elastic limit (m/m)	n	K(MPa)
DP780	594.4	200	960	0.00297	0.118	1228

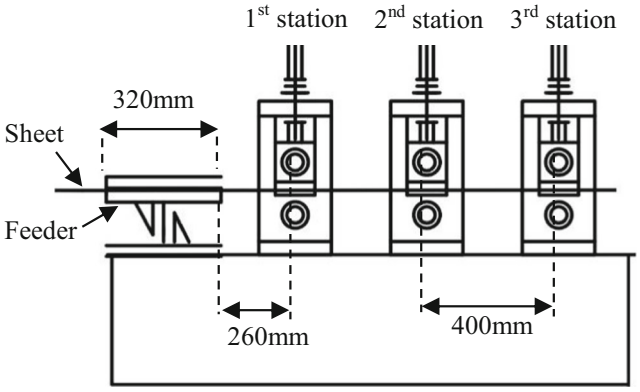

Fig. 2 Schematic of the roll forming set up

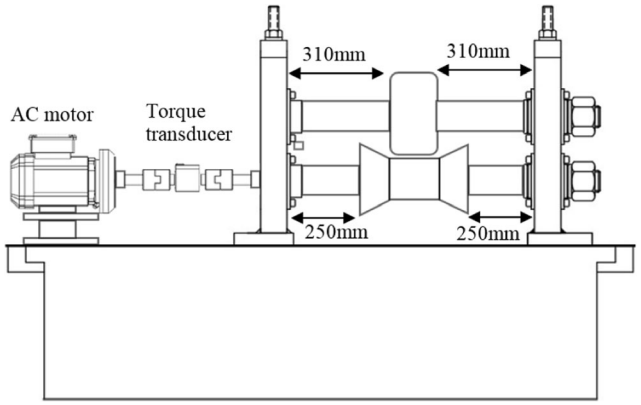

Fig. 4 Schematic of roll load and torque measurement in the 2nd station

This study will investigate the effect of material yield strength and hardening on the longitudinal bow as well as roll load and torque for the forming of a trapezoidal section. A regression analysis combined with Analysis of Variance (ANOVA) techniques is employed to establish the relationships between the process and material parameters and to determine their percentage influence on longitudinal bow, roll load and torque. The possibility of identifying the material properties of the incoming material and the resulting longitudinal bow of the section via the measurement of roll load and torque will be analysed with a practical example.

Experimental set up

A simple channel section was roll formed with Dual Phase 780 steel (DP780) in a laboratory roll former. The true stress strain curve of the DP780 steel determined in the standard tensile test ASTM E8/E8M [16] is given in Fig. 1a for samples directed 0, 45 and 90° to the rolling direction; the results show that the effect of planar anisotropy is small. The trues stress strain curve was converted into true stress-effective plastic strain and the Hollomon's power law (Eq. (1)) was fitted to the graph to determine the hardening parameters; hardening exponent (n) and strength coefficient (k). In Eq. (1), ε_{eps}, represents the effective plastic strain.

$$\sigma = k\varepsilon_{eps}{}^{n} \tag{1}$$

Reasonable correlation was achieved as shown in Fig. 1b and the material parameters are given in Table 1.

Strips that were 1000 mm in length, 150 mm in width and 2 mm in thickness were cut from a coil and roller levelled before roll forming to eliminate pre-existing residual stresses and to improve sheet flatness. The roll forming set up consists of three bottom roll driven roll stations and a feeder to feed the material into the first forming station as shown in Fig. 2.

The sheet was formed without lubrication with a line speed of 17.3*mm/s*. The forming sequence was 0º-20º-30º-free as shown in the flower pattern in Fig. 3a, and the constant radius bending technique was employed with a constant radius of 4.8 mm. In the constant radius method the segments of the arc element are bent into the final forming radius at each forming step while the arc length gradually increases as shown in Fig. 3b [17].

Roll load and torque were measured at the 2nd roll station by a shear web compression load cell and a rotation torque transducer [7] as shown in Fig. 4.

In this study the roll load was considered as the load exerted on the top shaft during the roll forming process and the roll torque was the torque exerted on the bottom roll during the operation. While in the first and the third station the roll gap was set according to the strip thickness (2 mm) in the 2nd station a roll gap 0.1 mm higher than the material thickness was chosen to avoid excessive loads on the equipment due to thickness variations [13].

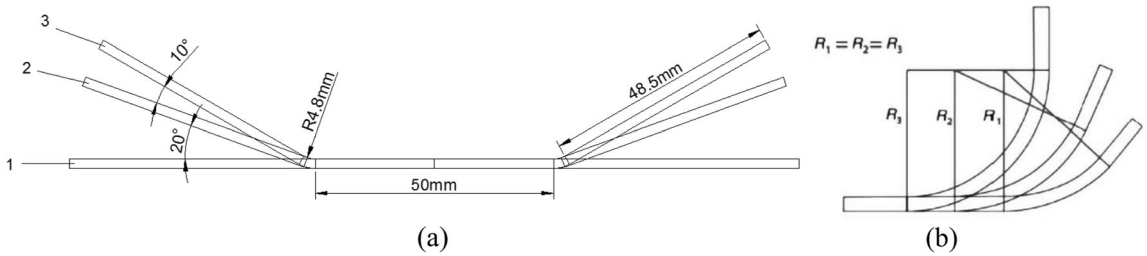

Fig. 3 (**a**) Flower pattern (**b**) Constant radius forming [17]

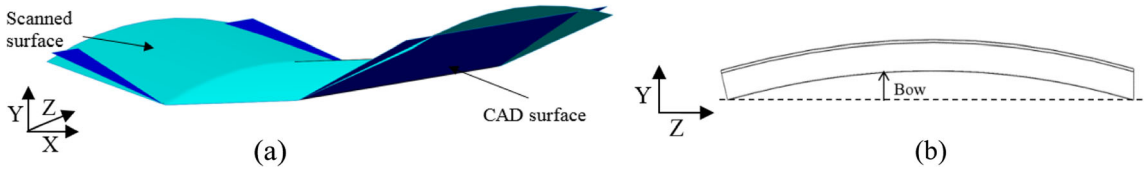

Fig. 5 (**a**) Alignment of the scanned part and the ideal CAD section through the part centre (**b**) Definition of bow

A new technique was introduced by the author to measure the longitudinal bow on the final roll formed parts. For this the outer surface of the roll formed part was scanned using the "ExaScan" 3D scanner [18] as shown in Fig. 5a. Black and white circular stickers, called targets, were pasted on the outer surface of the roll formed part and the background allowing the 3D scanner to identify the exact surface topology. Then the scanner was moved along the part until it captured the whole outer surface. The resolution of the scanned surface was 0.05 mm giving an accuracy of 0.04 mm. The scanned surface was then aligned with the ideal roll formed surface generated by Solidworks [19] as shown in Fig. 5a using the software package "Geomagic" [20]. The longitudinal cross section through the symmetric centre of the part was considered to evaluate bow. In this study longitudinal bow was defined as the vertical height deviation of the scanned part along the symmetric centre as shown in Fig. 5b. The symmetry line was chosen to maintain the consistency of the measurements.

Numerical analysis

Model set up

The commercial software package Copra RF/FEA [21] was applied for the process design and the numerical analysis. Copra FEA is based on MSC Marc and uses an explicit solver.

In previous numerical roll forming studies the forming rolls were considered as rigid and stationery bodies and deformation in the frame, the shafts, and the bearings was not taken into account [22–25]. This led to the overestimation of roll load and torque [26]. The numerical model applied in this study will account for the deflection of the shafts and frame components to enable the accurate analysis of roll load and torque similar to the approach employed by Groche et al. [27], which will be explained later. Figure 6 shows the numerical model applied in this investigation.

The coulomb friction model was adopted and the coefficient of friction between the strip and the rolls was assumed to be 0.1 [22, 28]. The forming rolls and the feeder were modelled as rigid bodies while the strip was defined as a deformable body generated from full integration, hexahedral, type 7 arbitrarily distorted brick elements available in the MSC MARC software element library [29]. Only one element through the strip thickness was chosen to minimise the computational time required. An analysis performed with two elements through the material thickness revealed an increase in roll load and torque by 5.8 % and 8.8 % respectively compared to the single element model. A similar trend with increasing number of elements through the material thickness has been observed in previous studies [27, 30].

The friction between the feeder and the strip was considered to be zero. The roll gap was set to be the same as the material thickness (2 mm) in the 1st and the 3rd station while it was adjusted to be 0.1 mm higher than the material thickness in the 2nd station corresponding to the experimental set up. The vertical upward force measured on the top roll in the second station and the torsion on the bottom roll correspond to the experimentally measured roll load and torque respectively. For that the vertical reaction force on the control node of the top roll was measured as the roll load and the torque applied on the bottom roll axis was measured as the roll torque. The rolls are fixed in space while the strip moves forward through the stations due to the frictional pulling force.

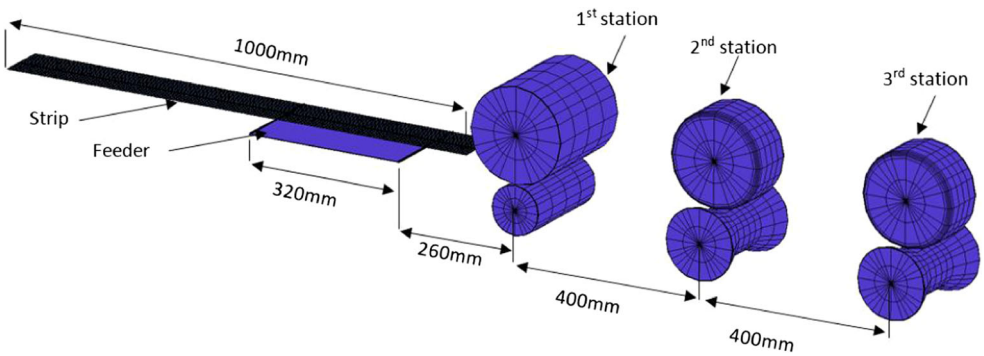

Fig. 6 Numerical model of the roll forming process

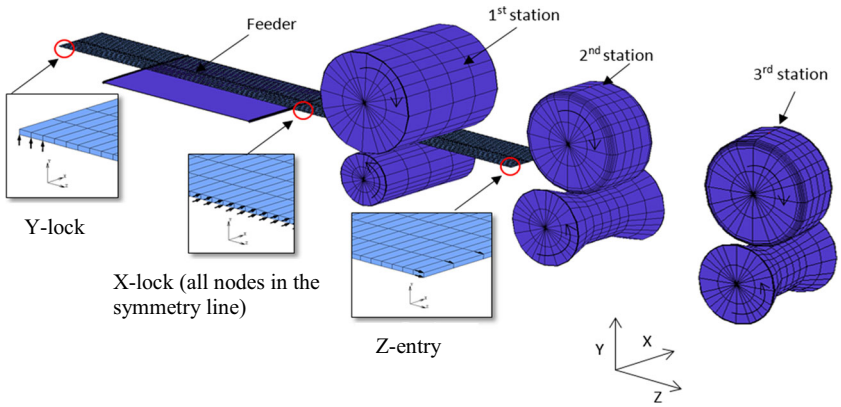

Fig. 7 Boundary conditions applied to the model of the roll forming process

Three boundary conditions were introduced as shown in Fig. 7. The X-lock boundary condition is applied to all nodes along the symmetric line of the part and restricts the material movement in X direction due to symmetry. The Y-lock is applied to the last three bottom nodes along the symmetry line and keeps the symmetry centre line at the same vertical position throughout the whole forming process. The Z-entry is applied to the first six top and bottom nodes from the symmetry corner and introduces a displacement in Z direction until the strip enters the first roll gap; then the strip moves forward due to the combined effect of frictional force between the strip and the rolls and the rotation of the top and bottom rolls. The rotational speed of the bottom roll was set to be 3.25 rpm giving a line speed of $17.3 mms^{-1}$ as in the experiments.

The elastic behaviour of the material was represented by the Hooke's stress–strain relationship given by Eq. (2). The Young's modulus, E, and the Poisson's ratio were taken as 200GPa and 0.3 respectively.

$$\sigma = E\varepsilon \tag{2}$$

Isotropic material behaviour was assumed and the von Mises yield criterion applied to define plastic material behaviour. For the verification of the numerical model with experimental roll forming results true stress-effective plastic strain data obtained for the DP780 material and fitted by the Hollomon's power equation (Fig. 1b) was used. For the parametric study a number of artificial true stress-effective plastic strain curves were developed and the procedure applied for this will be explained in more detail below.

Development of artificial material data

For this analysis, nine different artificial material properties were developed giving three levels of yield strength (Y) with three different hardening exponents (n) each. This enabled the detailed analysis of the interplay between material hardening and yield strength and the effect on roll load, torque and bow. The Hollomon's power law was applied for the artificial material data development. In the Hollomon's power law equation the strength coefficient (k) is a dependent variable that varies with the yield strength Y and the hardening exponent n. To generate true stress strain curves with distinct combinations of Y and n, k was determined for each material model based on the stress–strain relationship at the yield point (see Fig. 8). Based on Eq. (1) the strength coefficient, k , can be determined for each particular combination of Y and n using the relationship

$$k = \frac{Y}{{\varepsilon_0}^n} \tag{3}$$

where $\varepsilon_0 = \frac{Y}{E}$ is the strain corresponding to the yield strength.

The different combinations of yield strength and hardening exponents generated this way are shown in Fig. 9. The different yield strength levels and the hardening values are chosen to cover the Advanced High Strength Steel (AHSS) and UHSS grades commonly roll formed in the automotive industry. Those range from DP grades to martensitic steels which generally show high yield strength levels combined with very low material hardening.

Roll stand design

As mentioned above, in this study the stiffness of the main components of the roll forming station was taken into account.

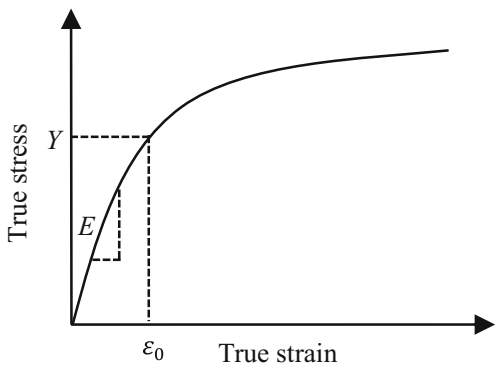

Fig. 8 Typical true stress–strain graph

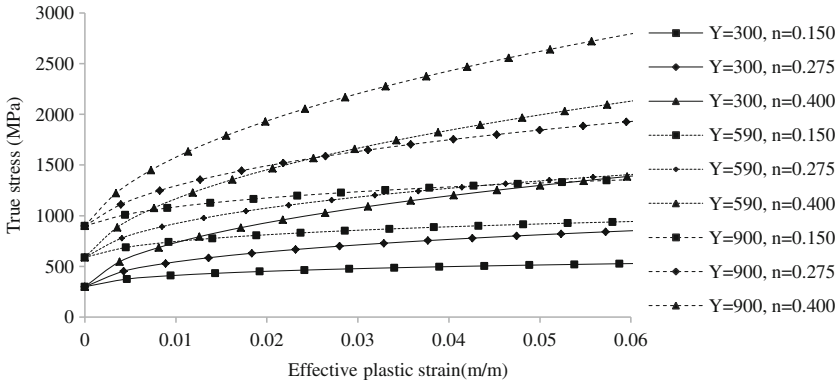

Fig. 9 Material input for the numerical models

To achieve this, first the loading behaviour of the main roll stand components, the top shaft, the bottom shaft and the frame components (see Fig. 10) was investigated. To determine their particular stiffness properties those three components were analysed separately. The resultant stiffness was introduced into the model which represents the summed up stiffness values of the top and bottom shafts and of the frame components.

For the stiffness analysis of the top and bottom shafts, half of the shaft was considered as in the numerical analysis only half of the strip is modelled due to part symmetry. The shafts were considered as cantilever beams that are fixed at one end. It was assumed that the shafts have a uniform cross section and that a point load is applied at the free end of the shaft due to the vertical forming force. The Frame consists of two columns, one arch, two frame connecting bolts and one adjustment bolt (Fig. 10). While the columns and the bolts can be assumed to be uniform bars under tensile load the arch is considered to be a fixed body supported at two ends and loaded at the centre. The formulas used to determine the stiffness are given in Table 2 together with the corresponding stiffness values. A Young's Modulus of E = 210GPa was assumed.

The overall stiffness of the frame including the shafts can then be calculated as follows;

$$k_{total} = \left(\frac{2}{k_1} + \frac{1}{2k_2} + \frac{1}{2k_3} + \frac{1}{k_4} + \frac{1}{k_5}\right)^{-1} \tag{4}$$

$$k_{total} = 31792\ N/mm$$

To introduce the stiffness obtained from Eq. (4) in the finite element model, a spring connection was introduced between the centre (control node) of the top shaft and a second node positioned vertically above the centre node as shown in Fig. 11. The stiffness of the spring was taken as the stiffness determined above for the whole frame (k_{total}) which was 31792 N/mm. The spring allows the top roll to move vertically to represent the deflection in the system as a result of the shaft and the frame components being deformed due to the roll load.

The total equivalent plastic strain introduced into the material is shown in Fig. 12 for roll stations 2 and 3. It can be seen that the highest equivalent plastic strain develops in the profile radius and is close to 0.03 for a forming angle of 30° in station 3 (Fig. 12b).

Model verification

The comparison between the numerical results and the roll load, torque and longitudinal bow analysed in the roll forming trials is shown in Fig. 13. It can be seen that the roll load is zero within the first 20 s until the sheet gets in contact with the rolls (Fig. 13a). Soon after that the strip reaches the roll gap and the roll load reaches its maximum value where it remains until the strip leaves the station. The experimental roll load is over estimated by the numerical model by 29 %. In the simulation only the stiffness of some frame and shaft components was considered. The estimation of the effect of the radial clearance of the self-aligning roller bearings and the stiffness

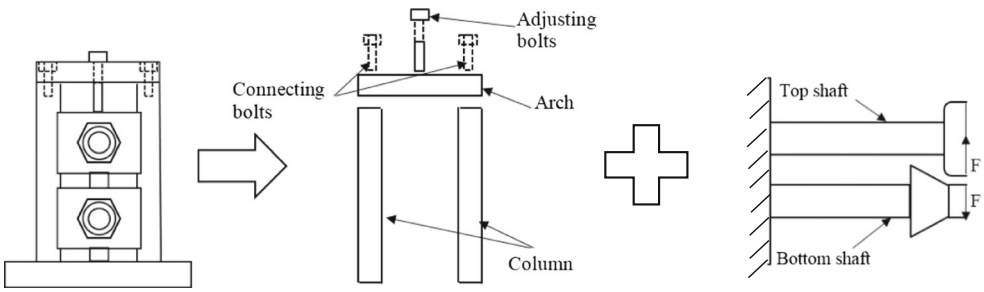

Fig. 10 Separation of the roll stand into shafts and frame components

Table 2 Frame stiffness components

Component	Dimensions	Stiffness formula	Stiffness(N/mm)
Roll shaft (k_1)	R=50.8 mm L=340 mm	$k = \frac{3EI}{L^3}$ Where I is the moment of inertia E is Young's modulus L is length	k_1=83839
Column(k_2)	40 mm×40 mm×400 mm	$k = \frac{AE}{L}$ Where A is cross sectional area	k_3=359189
Connecting bolts(k_3)	R=7 mm L=90 mm		k_4=431026 k_2=840000
Adjusting bolts(k_4)	R=7 mm L=150 mm		
Arch(k_5)	40 mm×50 mm×240 mm	$k = \frac{48EI}{L^3}$	k_5=303819

of the bearings and the bearing housings is difficult and therefore was not taken into account. The frictional force between the top shaft bearing housing and the columns may have influenced the experimental analysis of the roll load and may be, to some extent, the cause of the deviation observed in this study between the simulated and the experimentally measured roll load. For torque the maximum error of the numerical model is around 15.9 % (Fig. 13b). One of the reasons for this may be the underestimation of the coefficient of friction between the strip and the rolls which directly affects roll torque. Other authors proposed coefficients of frictions as high as 0.2 [5, 15]. The comparison between the numerical and the experimental results for longitudinal bow are shown in Fig. 13c. There is a good agreement between the numerical and experimental results for the maximum longitudinal bow. Overall, the results show that the current numerical model sufficiently represents the experimental set up.

Results and discussion

The values determined for longitudinal bow, roll load and torque applying the numerical model described above and the nine combinations of material yield strength and hardening exponent are shown in Table 3.

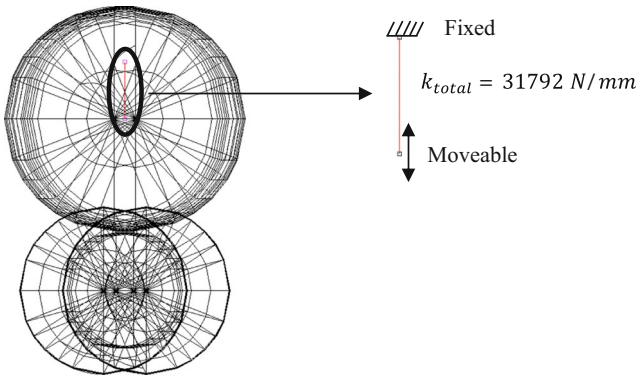

Fig. 11 Introduction of the shaft deflection in the model

Above results will be used in a regression analysis to determine their empirical relationships. Here the yield strength and the hardening exponent are considered as the input parameters while the longitudinal bow, roll load and torque are considered to be the output parameters. The relationship between the output parameters will also be established to determine the link between longitudinal bow, roll load and torque. The first order multiple linear regression model can be represented as

$$P_i = \beta_0 + \beta_1 x_1 + \beta_2 x_2 \tag{5}$$

where P_i represents the output parameters and x_1, x_2 are the yield strength, Y, and the hardening exponent, n, respectively. It is important to note that P_i is the dependent variable and x_1 and x_2 are independent variables; P_i, x_1 and x_2 therefore may not have the same dimensions. For the regression analysis the commercial software package MINITAB [31] was applied and the linear equations suggested are given in Table 4. The coefficient of determination (R^2_{adj}) is also shown and gives a measure for the accuracy of the suggested equation. Additionally to that the results of the variance analysis are given for each output variable in Table 5. The F value is another significant parameter which determines the degree of accuracy of a regression equation. According to the variance test results in Table 5, the suggested F value should be greater than F(2, 6) where 2 indicates the degree of freedom (DoF) of the regression model and 6 indicates the DoF of the residual error. The DoF defines the number of independent variables in a model. If the significance level, α is taken as 0.05 %, then F (2, 6) needs to be greater than 34.8 (this value is taken from the standard F statistic table) for the regression model to be of statistical significance. Therefore, considering the F values given in Table 5, the linear regression models can be accepted for longitudinal bow, load and torque as for those the F values are greater than 34.8. The P value determines if the model is statistically significant. This is the case if the P value is < α

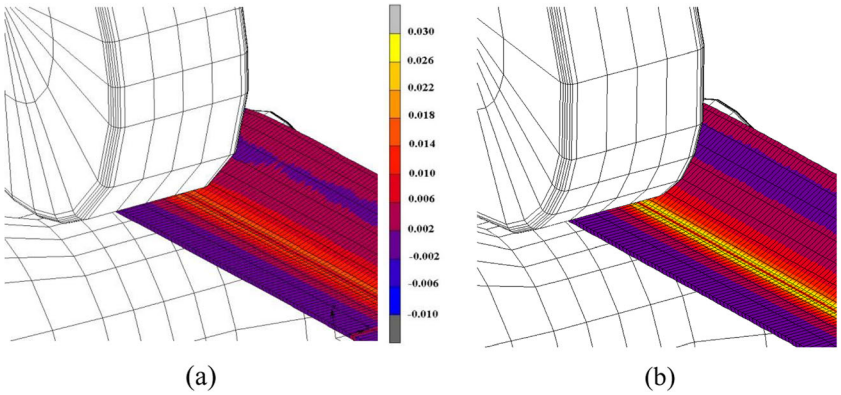

Fig. 12 Equivalent plastic strain distribution in the DP780 strip measured in (**a**) Station 2 (**b**) Station 3

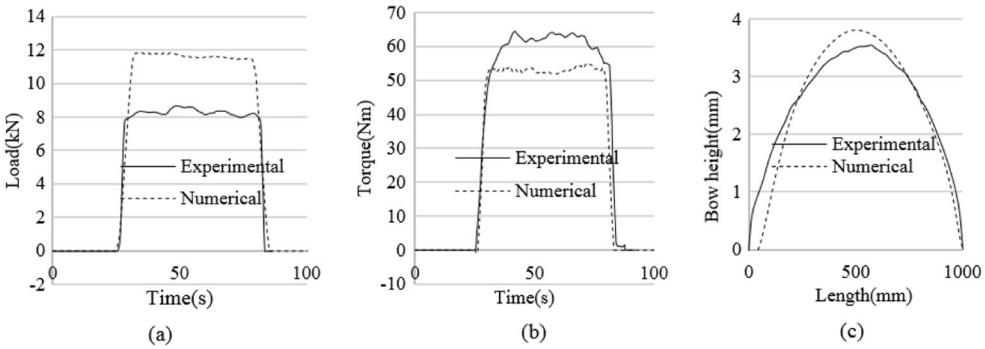

Fig. 13 Comparison between experimental and numerical results for (**a**) Roll load (**b**) Roll torque (**c**) Longitudinal bow

which is true for all parameters considered here as it is shown in Table 5.

The regression equations in Table 4 indicate a negative relationship between both yield strength and hardening exponent and longitudinal bow, i.e. longitudinal bow decreases with increasing yield strength and hardening exponent. In roll forming when the strip is bent in the roll forming station a point on the edge of the strip travels a longer distance compared to one positioned in the centre. This leads to the development of longitudinal strain in the edge and if its magnitude exceeds the elastic limit of the material, it is permanent. Such an imbalance in longitudinal strain between the strip edge and the centre results in bow [8]. When the yield strength is high the elastic limit of the material increases. This allows the material to longitudinally deform within the elastic limit during roll forming leading to a lower level of longitudinal bow [7, 15]. Some recent studies have shown that UHSS grades that show low material hardening deviate from this trend which may be due to their hardening behaviour [32]. The effect of the hardening on bow observed in this study is therefore important. After the material yields a high hardening exponent may restrict further permanent deformation in the material and through that may have a similar effect as that observed for an increase in material yield strength above. For roll load and

Table 3 Numerical results for longitudinal bow, roll load and torque

Model	*Y*(MPa)	*n*	Maximum Bow(mm)	Load(kN)	Torque(Nm)
Model 1	390	0.15	6.20	10.31	47.14
Model 2	390	0.25	5.62	12.54	59.04
Model 3	390	0.35	5.11	14.97	71.56
Model 4	590	0.15	3.82	11.99	54.24
Model 5	590	0.25	3.54	14.23	65.27
Model 6	590	0.35	3.12	16.73	77.80
Model 7	790	0.15	1.34	13.54	59.95
Model 8	790	0.25	1.42	15.77	71.33
Model 9	790	0.35	1.37	18.30	84.46

Table 4 Equations suggested by the regression analysis

Parameter	Equation	R^2_{adj}(%)
Maximum bow	10.5−0.0107 *Y*−2.93 *n*	98.4
Load	3.55+0.00816 *Y*+23.6 *n*	99.9
Torque	16.8+0.0317 *Y*+121 *n*	99.8

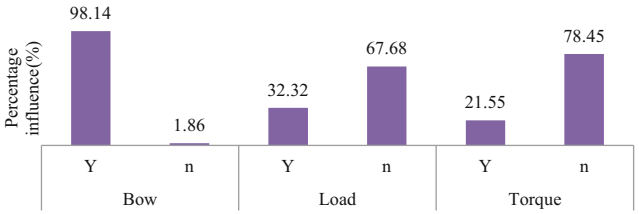

Fig. 14 Percentage influence of material properties on bow, roll load and torque

torque direct positive linear relationships with the yield strength and the hardening exponent are observed (Table 4). When the yield strength of the material is high the deformation energy needed to form the material increases [12] which leads to higher levels of roll load and torque. This was observed by several researchers in experimental and numerical studies [13, 26, 33]. However the effect of material hardening on roll load and torque has been unknown up to now. The area under the stress–strain curve increases with the hardening exponent, and this results in a higher deformation energy explaining the increase in roll load and torque with material hardening.

The percentage influence of material yield strength and hardening on longitudinal bow, roll load and torque is shown in Fig. 14. It becomes clear that longitudinal bow is almost entirely influenced by the material yield strength, rather than by material hardening. As mentioned above longitudinal bow is the result of permanent longitudinal deformation in the strip edge. Nevertheless, the magnitude of this permanent longitudinal edge strain is generally very low [34] leading to only minor material hardening. This explains the higher influence of material yield strength on longitudinal bow compared to material hardening.

In contrast to that the hardening exponent has a higher influence on roll load and torque compared to the material yield strength. The magnitude of roll load and torque are mainly related to the transverse bending of the part which is the main deformation mode in roll forming and generally high plastic strain levels are reached. According to the simple pure bending theory, the transversal bending strain in the outer surface of a bent strip can be calculated by the following relation [35].

$$\varepsilon_b = \frac{t}{2R} \tag{6}$$

where ε_b is the bending strain of the outer surface, t is the material thickness and R is the radius of the neutral axis. The final forming radius and bending angle of 4.8 mm and 30° respectively of the formed section (Fig. 3a) lead to a radius of curvature of the neutral axis $\frac{1}{R} = 0.172mm^{-1}$. This together with a material thickness of 2 mm results in an overall bending strain at the sheet outer fibre of ε_b=0.172. This is significantly higher than the elastic limit strain of the material (Fig. 1a and Table 1) and results in high material hardening during roll forming which explains the high effect of material hardening on the roll load and torque.

The linear regression analysis has been also applied to analyse if there is a relationship between the output parameters (bow, roll load and torque). Again the results obtained for the nine different material combinations given in Table 3 were applied to obtain a multiple regression model for longitudinal bow in terms of roll load and torque. According to that model, proposed by MINITAB, the longitudinal bow can be expressed as below.

$$\text{Bow} = 12.2 - 4.87\ \text{Load} + 0.925\ \text{Torque} \tag{7}$$

The corresponding coefficient of determination is R^2_{adj} = 95.6 %, which indicates a reasonable fit in the regression line. The corresponding ANOVA results are shown in Table 6

Table 5 Analysis of variance

Parameter	Source	DoF	Sum of squares	Mean squares	F	P
Bow	Model	2	27.789	13.894	251.98	0
	Residual error	6	0.331	0.055		
	Total	8	28.119			
Load	Model	2	49.446	24.723	3112.77	0
	Residual error	6	0.048	0.008		
	Total	8	49.494			
Torque	Model	2	1116.58	558.29	2589.43	0
	Residual error	6	1.29	0.22		
	Total	8	1117.88			

Table 6 Analysis of variance (ANOVA)-II

Parameter	Source	DoF	Sum of squares	Mean squares	F	P
Bow	Model	2	27.201	13.601	88.88	0
	Residual error	6	0.918	0.153		
	Total	8	28.119			

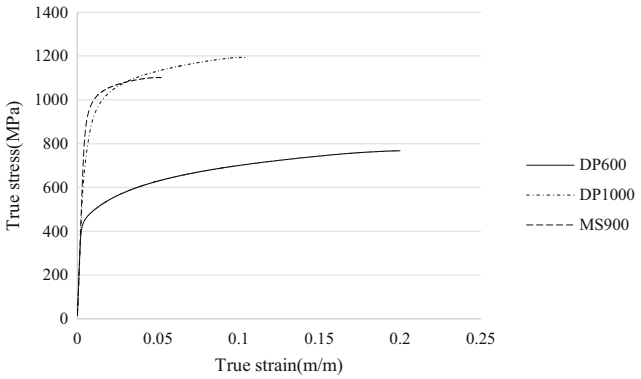

Fig. 15 Average true stress strain curves of the DP600, DP1000 and the MS900 steel

where the high magnitude of F confirms the significance of the model.

This suggests that for the roll forming process analysed here the relationship established in Eq. (7) can be applied to estimate the magnitude of bow if the roll load and torque are known and only the material properties are varied. This represents the conditions in the roll forming of automotive components from UHSS where the process set up remains the same while the yield strength and the hardening characteristics of the material change due to property variations from coil to coil.

Example

To verify the approach of predicting the magnitude of bow in the roll forming process based on the measurement of roll load and torque, the roll forming process set up of this study is numerically analysed for three different types of steel using the FEA model described above and the amount of bow measured. Additionally to that roll load and torque are determined. This is done for a DP600, a DP1000 and a MS900 steel which represent one AHSS and two UHSS respectively with distinct differences in yield strength and hardening characteristic. The average true stress strain curves of the three steel types analysed are shown in Fig. 15.

The values for roll load and torque predicted by the numerical analyses were applied to estimate the maximum magnitude of bow using Eq. (7). The comparison of the maximum bow estimated with Eq. (7) and the numerically determined values for bow are shown in Fig. 16.

While the DP600 and the DP1000 steel show positive values for bow, bow for the MS900 is in the opposite direction. Understanding this trend in detail is out of the scope of this investigation. It is clear that the longitudinal bow decreases with the increase in yield strength and after a certain yield strength, it becomes negative. For all three steel types a reasonable correlation is achieved (Fig. 16) between the maximum bow estimated with Eq. (7) and the bow predicted by the numerical model. The percentage error was 19.6 %, 3.25 % and 10.6 % for the DP600, the DP1000 and the MS900 steel respectively. This error can be reduced by introducing more simulations to this study which may lead to a more accurate regression model than developed here. However it is important to note that precise roll load and torque values are also needed to predict longitudinal bow in terms of roll load and torque more accurately.

Conclusion

The effect of material yield strength and hardening exponent on longitudinal bow as well as roll load and torque for the roll forming of a trapezoidal section is investigated using a numerical model. First the numerical set up is verified by experimental roll forming trials performed with DP780 steel. After that a regression analysis combined with Analysis of Variance

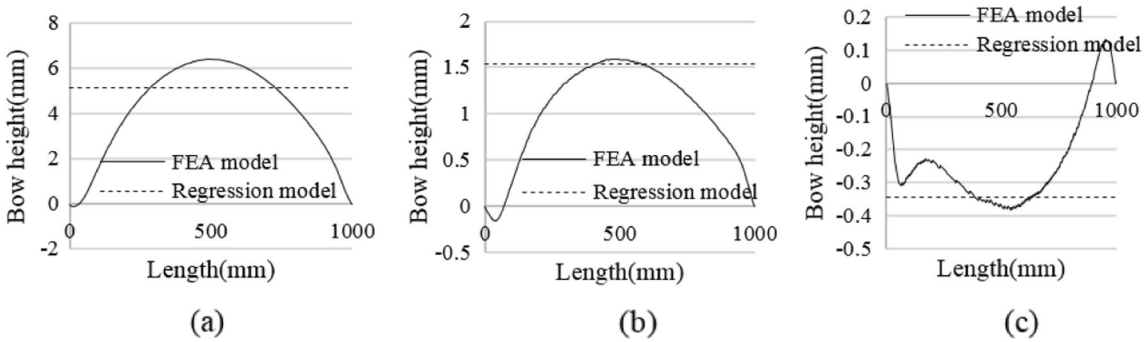

Fig. 16 Comparison of longitudinal bow estimated by Eq. (7) and predicted by the numerical model (**a**) DP600, (**b**) DP1000, (**c**) MS900

(ANOVA) techniques is employed to establish the relationships between the process and material parameters and to determine their percentage influence on longitudinal bow, roll load and torque. The analysis is performed for nine artificial true stress strain relationships representing three different levels of yield stress combined with three different hardening characteristics for each yield strength level. Major focus is on analysing the effect of yield strength and hardening exponent on bow, roll load and torque.

The results show that longitudinal bow has a linear negative relationship with the yield strength while the effect of material hardening is low. In contrast to that both roll load and torque have a linear positive relationship with the yield strength and the hardening exponent whereby the influence of material hardening is significantly higher compared to that of material yield.

Using multiple linear regression analysis a relationship between longitudinal bow and roll load and torque is developed that allows the estimation of bow for any given material if the process set up is kept constant. The functionality of the relationship is proven for a DP600, a DP1000 and a MS900 steel representing one AHSS and two UHSS respectively. Good correlation between the numerical predictions for bow and those estimated based on the developed relationship is observed. This suggests that for the particular roll forming set up presented here changes in bow due to the variation of material properties can be successfully estimated based on changes in roll load and torque determined in one forming station. The results of the current study represent a first step towards an in-line process control where changes in material parameters are estimated on the basis of roll load and torque and related to the final shape of the product. In combination with adjustable tooling or special shape compensation techniques this may allow the in-line compensation of shape defects in future roll forming lines.

Acknowledgments The authors appreciate the financial support of the Australian Research Council (ARC Linkage grant - LP120100111) and thank data M sheet metal solutions for providing several licences of Copra RF/FEA. The authors further would like to thank Emeritus Professor J.L. Duncan for his assistance in writing this paper and appreciate the support of Dr. Joseba Mendiguren, Mr. Ahmad Erfani and Mrs. Shiromani Desinghe.

References

1. Sweeney K, Grunewald U (2003) The application of roll forming for automotive structural parts. J Mater Process Technol 132:9–15
2. Yan PJ, Han JT, Jiang ZY, Li HJ, Liu LX (2011) Investigation of high strength steel for automotive roll-forming parts. Adv Mater Res 189:3001–3006
3. Troive L, Ingvarsson L (2008) Roll forming and the benefits of ultrahigh strength steel. Ironmak Steelmak 35:251–253
4. Weiss M, Marnette J, Wolfram P, Larrañaga J, Hodgson PD (2012) Comparison of bending of automotive steels in roll forming and in a V-die. Key Eng Mater 504:797–802
5. Badr OM, Rolfe B, Hodgson P, M. Weiss (2013) The effect of forming strategy on the longitudinal bow in roll forming of advanced high strength steel. In NUMISHEET 2014: The 9th International Conference and Workshop on Numerical Simulation of 3D Sheet Metal Forming Processes: Part A Benchmark Problems and Results and Part B General Papers, pp. 876–879
6. Halmos GT (2006) Roll forming handbook. Taylor & Francis, Boca Raton
7. Abeyrathna B, Rolfe B, Hodgson PD, Weiss M (2013) A first step towards in-line shape compensation for roll forming applications. Presented at the IDDRG 2013, Zurich, Switzerland
8. Kiuchi M (1999) Deformation characteristics of metal strips in roll forming. Presented at the Tubemaking for Asia's recovery : international conference, Singapore
9. De Souza T, Rolfe B (2008) Multivariate modelling of variability in sheet metal forming. J Mater Process Technol 203:1–12
10. Ona H, Jimma T, Fukaya N (1983) Experiments into the cold roll-forming of straight asymmetrical channels. J Mech Work Technol 8: 273–291
11. Groche P, Beiter P, Henkelmann M (2008) Prediction and inline compensation of springback in roll forming of high and ultra-high strength steels. 2, Production Engineering
12. Bhattacharyya D, Smith PD, Thadakamalla S, Collins I (1987) The prediction of roll load in cold roll-forming. J Mech Work Technol 14:363–379
13. Lindgren M (2007) Experimental investigations of the roll load and roll torque when high strength steel is roll formed. J Mater Process Technol 191:44–47
14. Sagström E, Swerea I, Lundberg M, Kimab S, Gustafson H, Bendiro A et al (2009) Roll forming of a hat-profile in UHSS – experimental study and FE-simulation. *LättUHS,* vol. Report 6
15. Azizitafti R, Weiss M, Naeini H.M., Tehrani MS (2012) The effect of material and geometric variables on the straightness of a roll formed channel. In International Conference on Advances in Materials and Processing Technologies, Wollongong
16. ASTM (2011) Standard test methods for tension testing of metallic materials
17. Tekkaya AE (2012) Sheet metal forming: processes and applications. Asm International
18. ExaScan 3D scanner. Available: http://www.creaform3d.com/en
19. Solidworks. Available: http://www.solidworks.com/
20. Geomagic Qualify. Available: http://www.geomagic.com/en/
21. COPRA® RF - Software for Roll Forming. Available: http://www.datam.de/en/products-solutions/roll-forming/
22. Lindgren M (2009) Experimental and computational investigation of the roll forming process. PHD Thesis, Division of Material Mechanics, Luleå University of Technology
23. Larranaga J (2011) Geometrical accuracy improvement in flexible roll forming process by means of local heating. PhD, Department of Mechanical and Industrial Production, Mondragon University
24. Paralikas J, Salonitis K, Chryssolouris G (2009) Investigation of the effects of main roll-forming process parameters on quality for a V-section profile from AHSS. Int J Adv Manuf Technol 44:223–237
25. Wiebenga JH, Weiss M, Rolfe B, van den Boogaard AH (2013) Product defect compensation by robust optimization of a cold roll forming process. J Mater Process Technol 213:978–986
26. Larrañaga J, Galdos L, Uncilla L, Etxaleku A (2010) Development and validation of a numerical model for sheet metal roll forming. Int J Mater Form 3:151–154
27. Groche P, Mueller C, Baeumer L (2014) Verification of numerical roll forming loads with the aid of measurement equipment. In Advanced Materials Research, pp. 373–380

28. Groche P, Mueller C, Traub T, Butterweck K (2013) Experimental and numerical determination of roll forming loads. Steel Research International
29. Marc® User Manual, ed: MSC Software Corporation, 2007
30. Hellborg S (2007) Finite element simulation of roll forming. Blech Rohre Profile 39:298–305
31. MINITAB software. Available: http://www.minitab.com/
32. Galdos L, Larranaga J, Uncilla L, Lete H, Arrixabalaga G (2009) Process simulation and experimental tests of cold roll forming of a u-channel made of different ultra high strength steel. Presented at the Rollform09. 1st international congress on roll forming
33. Davoodi B, Naeini HM, Asl YD, Azizi R, Kasaei TMM, Panahizadeh VR (2010) Numerical and experimental investigation of roll forces and torques in cold roll forming of a channel section, pp. 581–586
34. Abeyrathna BN, Rolfe B, Hodgson PD, Weiss M (2014) An experimental investigation of edge strain and bow in roll forming a V-section. Mater Sci Forum 773–774(2014):153–159
35. Hu J, Marciniak Z, Duncan J (2002) Mechanics of sheet metal forming: Butterworth-Heinemann